Title: Biomass burning emissions in north Australia during the early dry season: an overview of the 2014 SAFIRED campaign

Authors:

Marc D. Mallet[1], Maximilien J. Desservettaz[2], Branka Miljevic[1*], Andelija Milic[1], Zoran D. Ristovski[1], Joel Alroe[1], Luke T. Cravigan[1], E. Rohan Jayaratne[1], Clare Paton-Walsh[2], David W.T. Griffith[2], Stephen R. Wilson[2], Graham Kettlewell[2], Marcel V. van der Schoot[3], Paul Selleck[3], Fabienne Reisen[3], Sarah J. Lawson[3], Jason Ward[3], James Harnwell[3], Min Cheng[3], Rob W. Gillett[3], Suzie B. Molloy[3], Dean Howard[4], Peter F. Nelson[4], Anthony L. Morrison[4], Grant C. Edwards[4], Alastair G. Williams[5], Scott D. Chambers[5], Sylvester Werczynski[5], Leah R. Williams[6], V. Holly L. Winton[7,n], Brad Atkinson[8], Xianyu Wang[9], Melita D. Keywood[3*]

Affiliations:

[1]Department of Chemistry, Physics and Mechanical Engineering, Queensland University of Technology, Queensland, Brisbane, 4000, Australia

[2]Centre for Atmospheric Chemistry, University of Wollongong, Wollongong, New South Wales, 2522, Australia

[3]CSIRO Oceans and Atmosphere, Aspendale, Victoria, 3195, Australia

[4]Department of Environmental Sciences, Macquarie University, Sydney, New South Wales, 2109, Australia

[5]Australian Nuclei Science and Technology Organisation, Sydney, New South Wales, 2232, Australia

[6]Aerodyne Research, Inc., Billerica, Massachusetts, 01821, USA

[7]Physics and Astronomy, Curtin University, Perth, Western Australia, 6102, Australia

[8]Bureau of Meteorology, Darwin, Northern Territory, 0810, Australia

[9]National Research Centre for Environmental Toxicology, Brisbane, Queensland, 4108, Australia

[n]Now at the British Antarctic Survey, Cambridge, CB3 0ET, United Kingdom

***Corresponding Authors:**

Dr Melita Keywood

Contact Phone: +613 9239 4596

Contact Email: melita.keywood@csiro.au

Dr Branka Miljevic

Contact Phone: +61 7 3138 3827

Contact Email: b.miljevic@qut.edu.au

Keywords:

Biomass burning | savannah fires | greenhouse gases | aerosols | mercury

Abstract

The SAFIRED (Savannah Fires in the Early Dry Season) campaign took place from 29th of May, 2014 until the 30th June, 2014 at the Australian Tropical Atmospheric Research Station (ATARS) in the Northern Territory, Australia. The purpose of this campaign was to investigate emissions from fires in the early dry season in northern Australia. Measurements were made of biomass burning aerosols, volatile organic compounds, polycyclic aromatic carbons, greenhouse gases, radon, speciated atmospheric mercury, and trace metals. Aspects of the biomass burning aerosol emissions investigated included; emission factors of various species, physical and chemical aerosol properties, aerosol aging, micronutrient supply to the ocean, nucleation, and aerosol water uptake. Over the course of the month-long campaign, biomass burning signals were prevalent and emissions from several large single burning events were observed at ATARS.

Biomass burning emissions dominated the gas and aerosol concentrations in this region. Dry season fires are extremely frequent and widespread across the northern region of Australia, which suggests that the measured aerosol and gaseous emissions at ATARS are likely representative of signals across the entire region of north Australia. Air mass forward trajectories show that these biomass burning emissions are carried north west over the Timor Sea and could influence the atmosphere over Indonesia and the tropical atmosphere over the Indian Ocean. Here we present characteristics of the biomass burning observed at the sampling site and provide an overview of the more specific outcomes of the SAFIRED campaign.

1. Introduction

Tropical north Australia is dominated by savannah ecosystems. This region consists of dense native and exotic grasslands and scattered trees and shrubs. Conditions are hot, humid and wet in the summer months of December through March with hot, dry conditions for the rest of the year giving rise to frequent fires between June and November each year. Human settlements are relatively scarce in northern Australia, outside of the territory capital, Darwin (population of 146 000). To the north of the continent are the tropical waters of the Timor Sea, as well as the highly populated Indonesian archipelago. South of the savannah grasslands are the Tanami, Simpson and Great Sandy Deserts, spanning hundreds of thousands of square kilometers. Emissions from fires in the savannah regions of northern Australia are therefore the most significant regional source of greenhouse and other trace gases, as well as atmospheric aerosol. Globally, savannah and grassland fires are the largest source of carbon emissions from biomass burning(van der Werf et al., 2010;Shi et al., 2015) and play a significant role in the earth's radiative budget. It is therefore important to quantify, characterise and fully understand the emissions from savannah fires in northern Australia, taking into account the complexity, variability and diversity of the species emitted.

In Australia approximately 550 000 km^2 of tropical and arid savannahs burn each year (Meyer et al., 2012;Russell-Smith et al., 2007), representing 7% of the continent's land area. In the tropical north of Australia, the fires during the early dry season in May/June consist of naturally occurring and accidental fires, as well as prescribed burns under strategic fire management practice to reduce the frequency and intensity of more extensive fires in the late dry season in October and November (Andersen et al., 2005).

These fires in the early dry season burn with a low to moderate intensity and are normally confined to the grass-layer. Events where fires reach the canopy level are rare. These prescribed burns are an important process for the region and are undertaken by local landholders with permits, as well as government supported bodies and volunteers. There has been a recent push to reinstate traditional Aboriginal fire management regimes in this region (Russell-Smith et al., 2013). Other fire management regimes are implemented in similar environments around the world, such as the savannah ecosystems of Africa (Govender et al., 2006) or the chaparral grasses in the United States (Akagi et al., 2012). In general, fire management regimes are considered to benefit regional biodiversity and can lead to the long-term increase in living biomass, resulting in a reduction of greenhouse gas emissions (Russell-Smith et al., 2013). Quantifying the emissions from dry season fires on regional scales is essential for understanding the impact of these fires on the local and global atmosphere.

The components and concentrations of emissions from savannah fires are dependent upon the vegetation and burning conditions. While CO_2 is the primary product of biomass burning (BB), combustion processes also result in the emission of many other trace gases such as CO, CH_4, NOx, N_2O as well as non methane organic compounds (NMOCs) and aerosol particles composed of elemental carbon, organic carbon and some inorganic material (Crutzen and Andreae, 1990). The state of organics in biomass burning aerosols can vary significantly due to the type of plant material burned, the characteristics of the fires themselves as well as through aging processes in the atmosphere.

The effects of these emissions on radiative forcing are complex. The global average radiative forcing due to biomass burning aerosol-radiation interaction is estimated in the 5th International Panel on Climate Change report as 0.0 W m^{-2} with an uncertainty range of -0.20 to +0.20 Wm^{-2} (Bindoff et al., 2013). It is well known that greenhouse gases have a positive radiative forcing, heating up the atmosphere. Light absorbing carbon in the aerosol phase will also result in a positive radiative forcing (Jacobson, 2001) by absorbing shortwave radiation. Conversely, the presence of aerosol organic and inorganic matter can result in a negative radiative forcing by scattering solar radiation (Penner et al., 1998). In addition, biomass burning has been shown to be a significant source of cloud condensation nuclei (CCN), despite typically being composed of weakly hygroscopic substances (Lawson et al., 2015), due to the high number of particles emitted. This can result in a change in cloud droplet concentrations and volume, thereby influencing cloud formation, albedo and lifetime. The contribution of each species to the overall radiative forcing is also likely to change as smoke plumes age (Liousse et al., 1995). Furthermore, not all biomass burning aerosol will interact with radiation in the same way. For example, fresh BB emissions in the tropics has been observed to be more absorbing than those from boreal forest fires(Wong and Li, 2002). The role of biomass burning emissions is not limited to the Earth's radiative budget. Certain species of emissions (e.g., mercury) can be deposited and sequestered in soil (Gustin et al., 2008), vegetation (Rea et al., 2002) or bodies of water (LaRoche and Breitbarth, 2005).

Large-scale studies in Africa (Keil and Haywood, 2003), North America (Yokelson et al., 2009;Singh et al., 2006), Europe (Saarikoski et al., 2007), South America (Ferek et al., 1998) and Asia (Lin et al., 2013;Du et al., 2011) have provided valuable insight into

the impact of fire emissions on the regional atmosphere and laboratory measurements have proved to be useful in understanding the emission factors, composition and atmospheric processing of these emissions (Stockwell et al., 2014). Despite this, there is still a need for a better scientific understanding of the influence biomass burning has on atmospheric composition and air quality (Kaiser and Keywood, 2015), particularly around Australia. Furthermore, the tropics are disproportionately under-sampled and the atmospheric and ocean processes in these regions are of both regional and global consequence. The SAFIRED campaign will contribute towards better understanding biomass burning emissions and the atmospheric composition in tropical Australia.

On a more specific level, the SAFIRED campaign was undertaken with the following objectives:

- To obtain Australian savannah fire dry season emission factors for greenhouse gases, polycyclicaromatic hydrocarbons, gaseous elemental mercury, non-methane organic compounds, Aitken and accumulation mode aerosols and non-refractory submicron organic, sulfates, ammonia, nitrates and chlorides.
- To understand the emission of mercury from north Australian fires and to quantify the delivery of mercury to the ecosystem.
- To characterise the composition and size of aerosols in the region of north Australia and to understand the influence and extent of biomass burning on the total aerosol burden.
- To assess the ability of biomass burning aerosol to act as cloud condensation nuclei and to establish a link between aerosol composition, size and CCN.

- To assess the fractional solubility of aerosol iron and other trace metals in this region in the context of the potential supply of micronutrients required for marine primary production in the ocean.

2. Description of experiment

2.1 Site

The Australian Tropical Atmospheric Research Station (ATARS; 12°14'56.6"S, 131°02'40.8"E) is located on the Gunn Point peninsula in northern Australia (see Figure 1). ATARS is operated by the Australian Bureau of Meteorology and the CSIRO (Commonwealth Scientific and Industrial Research Organisation). Standard meteorological measurements (wind velocity, atmospheric pressure, precipitation) run permanently at ATARS and two laboratories are in place for the installation of other instruments. The SAFIRED campaign took place from 29th May 2014 until the 30th June 2014, with personnel and instruments from nine institutes utilising these laboratories to make comprehensive gaseous and aerosol measurements during this period of the early dry season.

2.2 Instruments and measurements

173 **Table 1 A summary of the quantities measured during SAFIRED and the respective instrument or measurement technique.**

174

Quantity	Instrument or Technique	Sample frequency	Reference
CO, CO_2, CH_4 and N_2O	Fourier transform infrared spectrometry	3 minute	(Griffith et al., 2012)
O_3	UV Photometric Ozone Analysis	1 minute	
Non methane organic compounds	Proton Transfer-Mass Spectrometry, high performance liquid chromatography of Supelco cartridge samples; gas chromatography of adsorbant tubes	3 minute; 12 hour; 12 hour	(Galbally et al., 2007); (Cheng et al., 2016); (Lawson et al., 2015)
Polycyclic aromatic hydrocarbons (gas and particle phase)	Gas chromatography and high resolution mass spectrometry of filter and foam samples	24 hour	(Wang et al., 2017)
Gaseous elemental mercury; gaseous oxidised mercury; and particulate-bound mercury	Cold vapour atomic fluorescence spectroscopy	5 minute; 2 hour; 2 hour	(Landis et al., 2002); (Steffen et al., 2008)
Radon	700L dual-flow two filter detector	1 hour	(Chambers et al., 2014)
Aerosol mobility size distributions (14 nm to 670 nm); neutral and charged aerosol size distributions (0.8 nm to 42 nm)	Scanning mobility particle sizer, Neutral cluster and air ion spectrometry	5 minute; 4 minute	(Mirme et al., 2007)
Cloud condensation nuclei concentration (at 0.5% supersaturation)	Supersaturated streamwise continuous-flow of aerosols in a wetted column using thermal-gradient followed by Optical Particle Counting of activated CCN	10 second	(Gras et al., 2007)
Elemental and organic carbon; water soluble ions; and anhydrous sugars (PM1 and PM10)	β+ attenuation; ion chromatography; high performance anion-exchange chromatography	12 hour	(Chow et al., 2007b); (Iinuma et al., 2009)
Soluble and total fraction of trace metals (PM10)	High-resolution inductively coupled plasma mass spectrometry analysis of extracted leachates and digests.	24 hour	(Winton et al., 2016)
Non-refractory chemical composition (PM1)	Time-of-flight aerosol mass spectrometry	3 minute	(Drewnick et al., 2005)
Aerosol volatility and hygroscopicity (50 nm and 150 nm)	Volatility and hygroscopicity tandem differential mobility analysis	12 minute (full cycle)	(Johnson et al., 2004)

2.2.1 Trace Gases

Greenhouse gases

Continuous measurement of CO_2, CO, CH_4 and N_2O were made using a high precision FTIR trace gas and isotope Spectronus analyser, developed by the Centre for Atmospheric Chemistry at the University of Wollongong. The analyser combines a Fourier Transform Infrared (FTIR) Spectrometer (Bruker IRcube), a pressure and temperature controlled multi-pass cell and an electronically cooled mercury cadmium telluride detector. A detailed description of the instrument and concentration retrieval technique are available in Griffith et al. (2012) and Griffith (1996).

Ozone and other trace gases

A Multi Axis Differential Optical Absorption Spectrometer (MAX-DOAS) was installed on the top of one of the laboratories during the campaign. The technique has been shown to provide the vertical profile of nitrogen dioxide, ozone, sulfur dioxide, formaldehyde, glyoxal and aerosol extinction (Sinreich et al., 2005;Honninger et al., 2004). The MAX-DOAS instrument used in this campaign was designed and built at the University of Wollongong. It consists of a vertically rotating prism capturing scattered solar radiation at different angles (1°, 2°, 4°, 8°, 16°, 30° and a reference at 90°) into a fibre optic that carries the radiation to a UV-Visible spectrometer (AvaSpec – ULS3648). Furthermore, a Thermo Scientific model 49i UV Photometric Ozone analyser was used to measure ozone concentrations.

Non-methane organic compounds

Online NMOC measurements were made using a high sensitivity Proton Transfer Reaction-Mass Spectrometer (PTR-MS; Ionicon Analytik) using H_3O^+ as the primary ion. The inlet was 10 m in length and drew air at 5 L min^{-1} from 2 m above the roof (approx 5.5 m above ground level). The PTR-MS ran with inlet and drift tube temperature of 60 ºC, 600 V drift tube, and 2.2 mbar drift tube pressure, which equates to an energy field of 135 Td. The PTR-MS sequentially scanned masses 15-190, with 1 second dwell time. The PTR-MS operated with the aid of auxiliary equipment which regulates the flow of air in the sample inlet and controls whether the PTR-MS is sampling ambient or zero air or calibration gas (Galbally et al., 2007).

Furthermore, AT VOC (adsorbent tube Volatile Organic Compounds) samples were collected by an automatic VOC sequencer which actively draws air through two multi-adsorbent tubes in series (Markes Carbograph 1TD / Carbopack X). The adsorbent tubes were then analysed by a PerkinElmer TurboMatrix™ 650 ATD (Automated Thermal Desorber) and a Hewlett Packard 6890A gas chromatography (GC) equipped with a Flame Ionization Detector (FID) and a Mass Selective Detector (MSD) at CSIRO Oceans and Atmosphere laboratories. Further details of the sampling and analyses are given in Cheng et al. (2016).

During sampling, carbonyls and dicarbonyls were trapped on S10 Supelco cartridges, containing high-purity silica adsorbent coated with 2,4-dinitrophenylhydrazine (DPNH), where they were converted to the hydrazone derivatives. Samples were refrigerated immediately after sampling until analysis. The derivatives were extracted from the cartridge in 2.5 mL of acetonitrile and analysed by high performance liquid

chromatography with diode array detection. The diode array detection enables the absorption spectra of each peak to be determined. The difference in the spectra highlights which peaks in the chromatograms are mono- or dicarbonyl DNPH derivatives and, along with retention times, allows the identification of the dicarbonyls glyoxal and methylglyoxal. Further details can be found in Lawson et al. (2015).

PAHs

PAHs were sampled through a high-volume air sampler (Kimoto Electric Co., LTD.) using a sampling rate typically at ~60 m^{-3} h^{-1}. The sampling rate was calibrated using an orifice plate prior to the sampling campaign and the sampling volume was calculated based on the calibrated sampling rate and sampling duration. A bypass gas meter installed on the sampler was used to monitor any anomalous fluctuation of the sampling rate during the sampling period. Particle-associated and gaseous PAHs were collected on glass fibre filters (Whatman™, 203×254 mm, grade GF/A in sheets) and subsequent polyurethane foam plugs respectively. The glass fibre filters and polyurethane foam, along with the field blank samples, were extracted separately using an Accelerated Solvent Extractor (Thermo Scientific™ Dionex™ ASE™ 350) after being spiked with a solution containing 7 deuterated PAHs (i.e. $^{2}D_{10}$-phenanthrene, $^{2}D_{10}$-fluoranthene, $^{2}D_{12}$-chrysene, $^{2}D_{12}$-benzo[b]fluoranthene, $^{2}D_{12}$-BaP, $^{2}D_{12}$-indeno[1,2,3-cd]pyrene, $^{2}D_{12}$-benzo[g,h,i]perylene) at different levels as internal standards for quantification purposes. Concentrated extracts were cleaned up by neutral alumina and neutral silica. Eluents were carefully evaporated to near dryness and refilled with 250 pg of $^{13}C_{12}$-PCB (polychlorinated biphenyl) 141 (in 25 µL isooctane) employed as the recovery/instrument standard for estimating the recoveries of the spiked internal standards and monitoring the performance of the analytical instrument. Samples were analysed using a Thermo Scientific™ TRACE™ 1310 gas chromatograph coupled to

a Thermo Scientific™ double-focusing system™ Magnetic Sector high resolution mass spectrometer. The HRMS was operated in electron impact-multiple ion detection mode and resolution was set to ≥ 10,000 (10% valley definition). An isotopic dilution method was used to quantify 13 PAH analytes including phenanthrene, anthracene, fluoranthene, pyrene, benzo[a]anthrancene, chrysene, benzo[b]fluoranthene, benzo[k]fluoranthene, benzo[e]pyrene, BaP, indeno[1,2,3-cd]pyrene, dibenzo[a,h]anthracene, benzo[g,h,i]perylene.

Mercury

Total gaseous mercury, gaseous elemental mercury + gaseous oxidised mercury (TGM; GEM + GOM), was sampled from a 10 m mast and measured via gold pre-concentration and cold vapour atomic fluorescence spectroscopy using a Tekran 2537X instrument. Simultaneously, GEM, GOM and Particulate-bound mercury (PBM) were individually measured using a Tekran 2537B connected to a combined Tekran 1130/1135 speciation unit sampling at a 5.4 m height. The sampling train of the 1130/1135 collects first GOM (KCl-coated denuder) then PBM (quartz wool pyrolyser) in series from a 10 L min^{-1} sampling flow, allowing GEM only to flow onwards for detection by subsampling by the 2537B. Due to the small atmospheric concentrations of GOM and PBM, pre-concentration occurred over a 1-hour period with subsequent analysis taking an additional hour. Continuous measurements of GEM at 5-minute resolution were made possible for the 2537B unit by rotating pre-concentration/analysis roles of the two internal gold traps. Both 2537 units sampled at 1 L min^{-1} and were calibrated every 23 hours using an internal mercury permeation source. For more information on the 2537 and 1130/1135 systems see Landis et al. (2002) and Steffen et al. (2008).

GEM fluxes were measured using the methods outlined in Edwards et al. (2005). Air samples were drawn at heights of 5.2 and 8.0 m through 46.4 m of nylon tubing using a PTFE diaphragm pump operating at 10 L min^{-1}. Subsampling from this flow through a 0.2 µm PTFE filter at 1 L min^{-1} by a Tekran 2537A, and switching between sample intakes, allowed resolution of a GEM gradient every 30 minutes. The transfer velocity was measured using a Campbell Scientific CSAT3 sonic anemometer and LI-COR 7200 closed path infrared gas analyser for CO_2, both located on the same tower as the gradient intakes at 6.6 m and sampling at 20 Hz.

Radon

In order to measure Radon concentrations, a 700 L dual-flow-loop two-filter radon detector, designed and built by the Australian Nuclear Science and Technology Organisation (Whittlestone and Zahorowski, 1998;Chambers et al., 2014), was installed at the ATARS in 2011 and has been fully operational since July 2012. The detector provided continuous hourly radon concentrations for the duration of the SAFIRED campaign, sampling air at 40 L min^{-1} from 12 m above ground level through 25 mm high-density polyethylene agricultural pipe. A coarse aerosol filter and dehumidifier were installed "upstream" of the detector, as well as a 400 L delay volume to ensure that thoron (^{220}Rn, half-life 55 s) concentrations in the inlet air stream were reduced to less than 0.5 % of their ambient values. The detector's response time is around 45 minutes, and the lower limit of detection is 40 - 50 mBq m^{-3}. Calibrations are performed on a monthly basis by injecting radon from a PYLON 101.15±4% kBq Ra-226 source (12.745 Bq min^{-1} ^{222}Rn), traceable to NIST standards, and instrumental background is checked every 3 months. In post processing, half-hourly raw counts were integrated to hourly values before calibration to activity concentrations (Bq m^{-3}).

2.2.2 Aerosols

Aerosol Drying System

An Automated Regenerating Aerosol Diffusion Dryer (ARADD) is permanently installed on the roof of the laboratory containing the aerosol instrumentation for this campaign. This was used in front of the aerosol manifold to continuously dry the aerosol sample. The ARADD design, similar to that described by Tuch et al. (2009), continuously conditions the aerosol sample to a relative humidity of below 40% with maximum aerosol transmission efficiency. The ARADD utilizes two diffusion drying columns in parallel, each containing 7 stainless steel mesh tubes of 10 mm internal diameter and approximately 800 mm length, surrounded by a cavity packed with silica gel. The aerosol sampled is directed into one column at a time, while the other column is regenerated by an ultra-dry compressed air system. All flows are controlled by software that directs sample flow and compressed air flow to the appropriate column with a series of valves. The ARADD has total suspended particulate style intake at the inlet of the aerosol sample path. This is a non-size-selective stainless-steel inlet with a semi-cicular hat over an inverted conical funnel of variable pitch ending with a 3/4" stainless-steel tube. In practise, the aerosols collected have an equivalent aerodynamic diameter of 100 μm or less depending on sampling conditions. The inlet led to a sample manifold at the exit of the system to provide sampling take-offs for the various aerosol instruments connected to the ARADD. Flow through the ARADD is provided by the instruments and pumps connected downstream. The ambient and inlet relative humidity for the entire sampling period were logged and are displayed in Supplementary Figure S1.

Aerosol Size

Aerosol size distributions were measured with a Scanning Mobility Particle Sizer (SMPS). A TSI 3071 long-column electrostatic classifier with a TSI 3772 Condensation Particle Counter (CPC) measured the size distribution over a range of 14 nm to 670 nm at a scan interval of 5 minutes.

In addition to the aerosol size distributions measured by the SMPS, neutral and charged aerosol particle distributions from 0.8 nm to 42 nm were measured using a Neutral cluster and Air Ion Spectrometer (NAIS)(Manninen et al., 2009;Mirme et al., 2007). In this study, the NAIS was set to operate in a cycle of 4 min including ion and neutral particle sampling periods of 2 and 1 minute, respectively, with the remaining minute being an offset period which is required to neutralize and relax the electrodes. The total sampling air flow was 60 L min^{-1}, the high flow rate being used to minimize ion diffusion losses and maximize the measured ion concentration sensitivity. Ion losses are accounted for during post-processing of the data by the software (Mirme et al., 2007).

Aerosol Composition and Water Uptake

PM_1 and PM_{10} 12-hour filter samples (night and day) were collected on a TAPI 602 Beta plus particle measurement system (BAM). Portions of the PM_1 filters have been analysed for elemental and organic carbon mass loadings using a DRI Model 2001A Thermal-Optical Carbon Analyzer following the IMPROVE-A temperature protocol (Chow et al., 2007b). Additional portions of the PM_1 filters were extracted in 5 ml of 18.2 mΩ de-ionized water and preserved using 1% chloroform. These extracts have been analysed for major water-soluble ions by suppressed ion chromatography and for

anhydrous sugars including levoglucosan by high-performance anion-exchange chromatography with pulsed amperometric detection (Iinuma et al., 2009).

Daily aerosol filters were collected using two Ecotech 3000 high-volume volumetric flow controlled aerosol samplers with PM_{10} size selective inlets. One high-volume sampler was used to collect aerosols on acid cleaned Whatman 41 filters to determine the soluble and total fraction of trace metals. Soluble trace metals were extracted from a filter aliquot using ultra-pure water (>18.2 mΩ) leaching experiments. Total trace metal concentrations were determined by digesting a second filter aliquot with concentrated nitric and hydrofluoric acids. Leachates and digested solutions were analysed by high resolution inductively couple plasma mass spectrometry. The second sampler was used to collect a set of aerosol samples on quartz filters for elemental and organic carbon analysis following (Chow et al., 2007a), and major anion and cation analysis.

The volatility and hygroscopicity of 50 nm and 150 nm particles were measured with a custom built Volatility and Hygroscopicity Tandem Differential Mobility Analyser (VH-TDMA). Inlet dried particles were size selected (alternating between 50 and 150 nm) using a TSI 3080 electrostatic classifier. Scans alternated between two different sample pathways. In the first, after size selection, particles were passed through a thermodenuder set to 120°C. The sample line was then split so that half went to an SMPS comprised of a TSI 3080 classifier and a TSI 3010 CPC (V-TDMA). The rest of the sample was passed through a humidifying system that exposed the particles to a relative humidity of 90% before being brought into another SMPS with a 3080 classifier and 3010 CPC (H-TDMA). Alternatively, the thermodenuder was bypassed in every

second scan so that the V-TDMA was used to verify the size selection and the H-TDMA was able to observe the hygroscopic growth of ambient particles. Each scan ran for 3 minutes, giving a full set of data every 12 minutes.

The chemical composition and properties of non-refractory sub-micron particles were investigated with a compact Time-of-Flight Aerosol Mass Spectrometer (cToF-AMS, Aerodyne Research, Inc.) and a Time of Flight Aerosol Chemical Speciation Monitor (ToF-ACSM, Aerodyne Research, Inc.). Both of these instruments operate with the same principle and have many identical components. An aerodynamic lens in the inlet of each instrument focuses the particles into a beam and differential pumping removes most of the gas phase. Particles are flash vaporized at 600°C and ionized by electron impact before passing through a time-of-flight mass spectrometer to a multi-channel plate detector in the cToF-AMS and a dynode detector in the ToF-ACSM. The cToF-AMS has the added benefit of having a particle Time-of-Flight (pToF) mode, which allows the size resolved chemical composition to be measured. Both instruments sampled through a $PM_{2.5}$ inlet and nafion dryer. In addition, the inlet of the cToF-AMS was incorporated into the VH-TDMA system, so that when the VH-TDMA was measuring ambient particles, the cToF-AMS would draw particles through the thermodenuder set at 120°C and vice-versa. This gives additional information about the chemical composition of the volatile component of submicron particles.

The number of particles activated to cloud droplets were measured using a Continuous-Flow Steam Wise Thermal Gradient Cloud Condensation Nuclei Counter (CCNC) from Droplet Measurement Technologies Inc. (DMT, model No. 100). Particles were

exposed to a 0.5% supersaturation and activated particles greater than 1μm were counted with an Optical Particle Counter using a 50 mW, 658 nm laser diode.

Back trajectories

Hourly 10-day air mass back trajectories terminating at ATARS were produced using the NOAA HYSPLIT model (Draxler and Rolph, 2003), and catalogued in a data base for use with the SAFIRED campaign data set. Global Data Assimilation System input files with 0.5° resolution were obtained from NOAA ARL FTP site (http://ready.arl.noaa.gov/gdas1.php) to drive the HYSPLIT model.

Satellite detection of fires

Data on the location of fires was collected from the Australian national bushfire monitoring system, Sentinel Hotspots. Hotspot locations are derived from the Moderate Resolution Imaging Spectroradiometer (MODIS) sensors on the Terra and Aqua satellites and the Visible Infrared Imaging Radiometer Suite (VIIRS) sensor on the Suomi NPP satellite. The Terra, Aqua and Suomi NPP satellites fly over the region around ATARS at approximately 10:30 am, 3 pm and 2:30 pm, respectively. Detection of fires is therefore limited to those that are flaming during these times.

3. Overview of Campaign

Fires and air masses

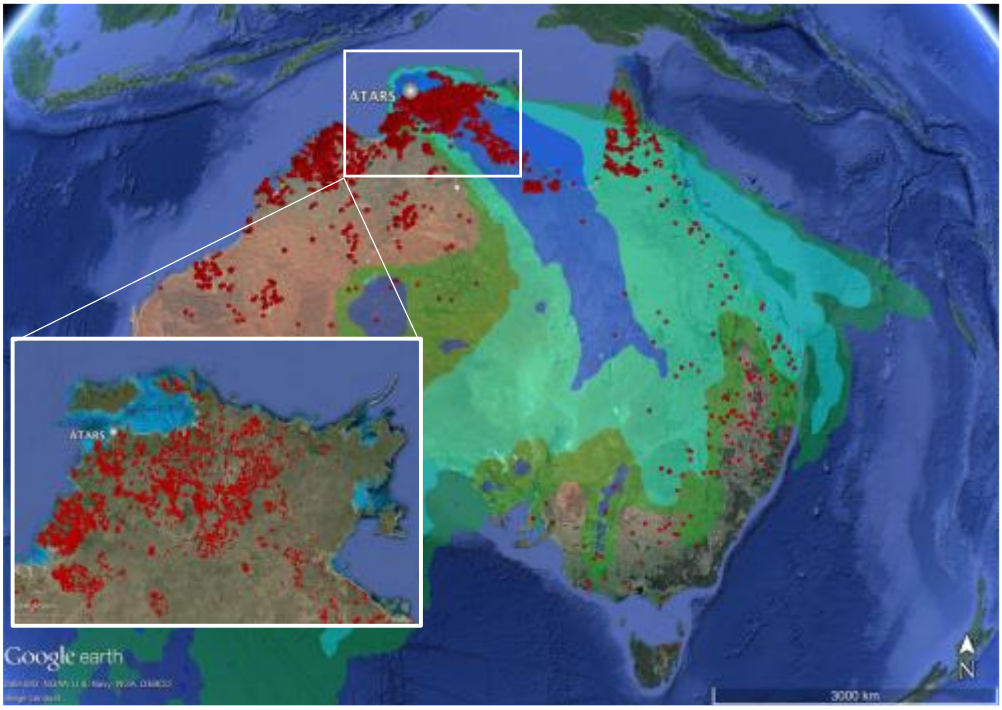

Figure 1 All satellite-detected fires with >50% detection confidence in June 2014 in Australia. Trajectory densities are shown as shaded regions (blue - >10% of all data; cyan - >1% of all data; green - >0.1% of all data)

Thousands of fires were observed in during the period of the SAFIRED campaign in Australia by the MODIS and VIIRS sensors on the Terra and Aqua NASA satellites. The vast majority of these occurred in the savannah regions of northern Australia. Over 28000 fires were detected within 400 km of ATARS during the sampling period. . Airmass back trajectories from the sampling site show that air masses over the study period predominately originated from the southeast (see Figure 1), generally over the regions where fires were frequently detected. Considering the daily satellite observations of close and distant fires, as well as meteorological, gaseous and aerosol measurements over the duration of SAFIRED, five periods were distinguished; four biomass burning related periods (BBP1, BBP2, BBP3 and BBP4) and a "coastal" period (CP). The dates for these periods are displayed in Table 2.

Table 2 The start and end dates for the four identified Biomass Burning Periods (BBP1, BBP2, BBP3 and BBP4) and the Coastal Period (CP).

Period	Start date (mm/dd/yy hh:mm)	End date (mm/dd/yy hh:mm)
BBP1	05/30/14 00:00	05/31/14 23:59
BBP2	06/06/14 00:00	06/12/14 23:59
BBP3	06/14/14 00:00	06/17/14 23:59
CP	06/19/14 12:00	06/22/14 23:59
BBP4	06/23/14 00:00	06/28/14 23:59

The number of detected fires on each day within 10 km, 20 km, 50 km, 100 km and 200 km of the sampling location was determined (see Figure 2). Several fires within 10 km were detected on the 30th of May (BBP1), the 9th and 10th of June (BBP2) and the 25th and 26th of June (BBP4). BBP1, BBP2 and BBP4 were also associated with the highest concentrations of most of the measured gaseous (Figure 3) and aerosol species (Figure 4). The periods between the 12th and 23rd of June (BBP3 and CP) had very few detected fires within 50 km of the station, corresponding to smaller gaseous and aerosol concentrations.

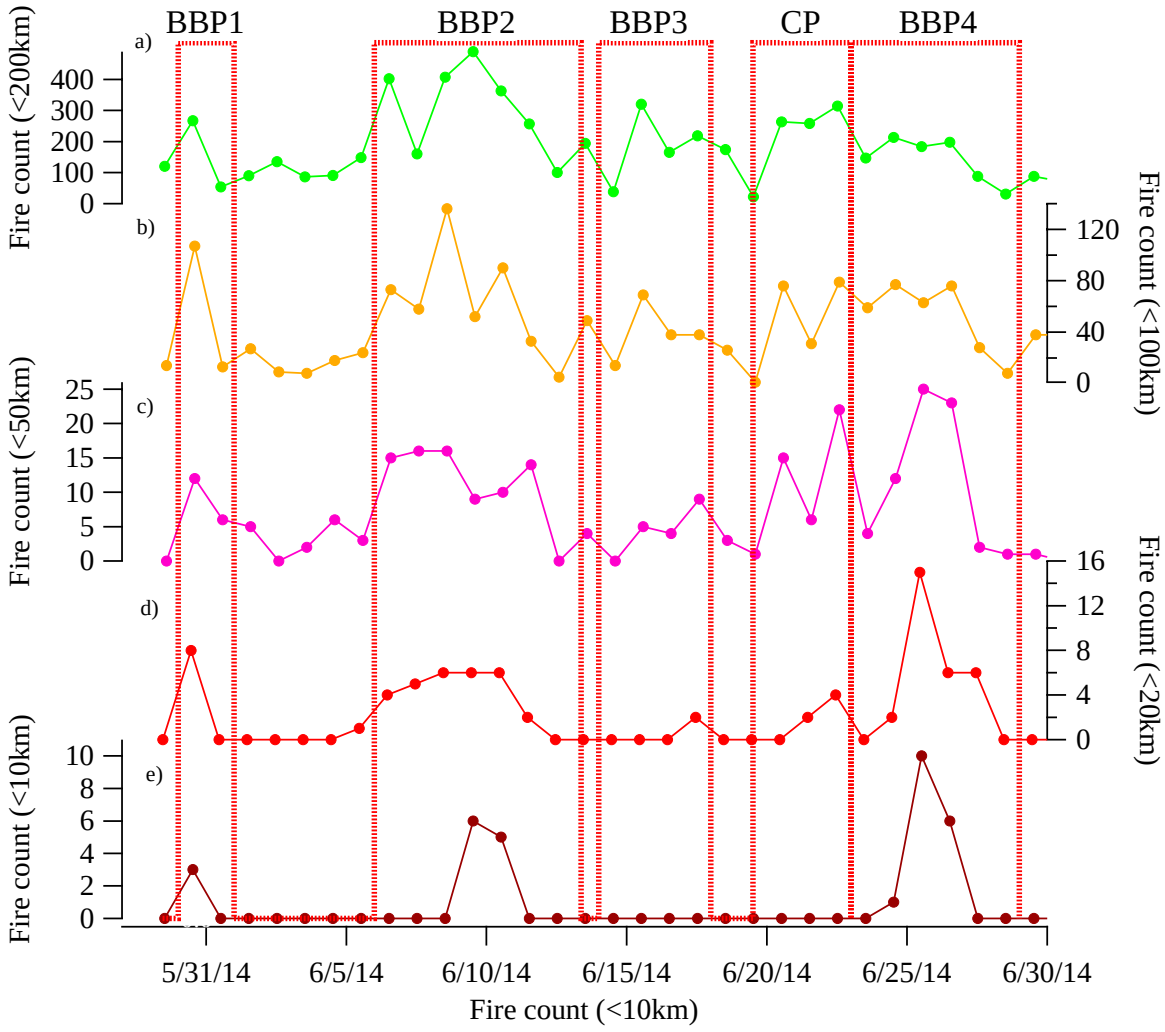

435

436 **Figure 2 The number of hotspots observed each day within (a) 200 km, (b) 100 km, (c) 50 km, (d) 20 km and**
437 **(e) 10 km of the ATARS, as detected by the MODIS and VIIRS sensors on the Terra and Aqua satellites.**

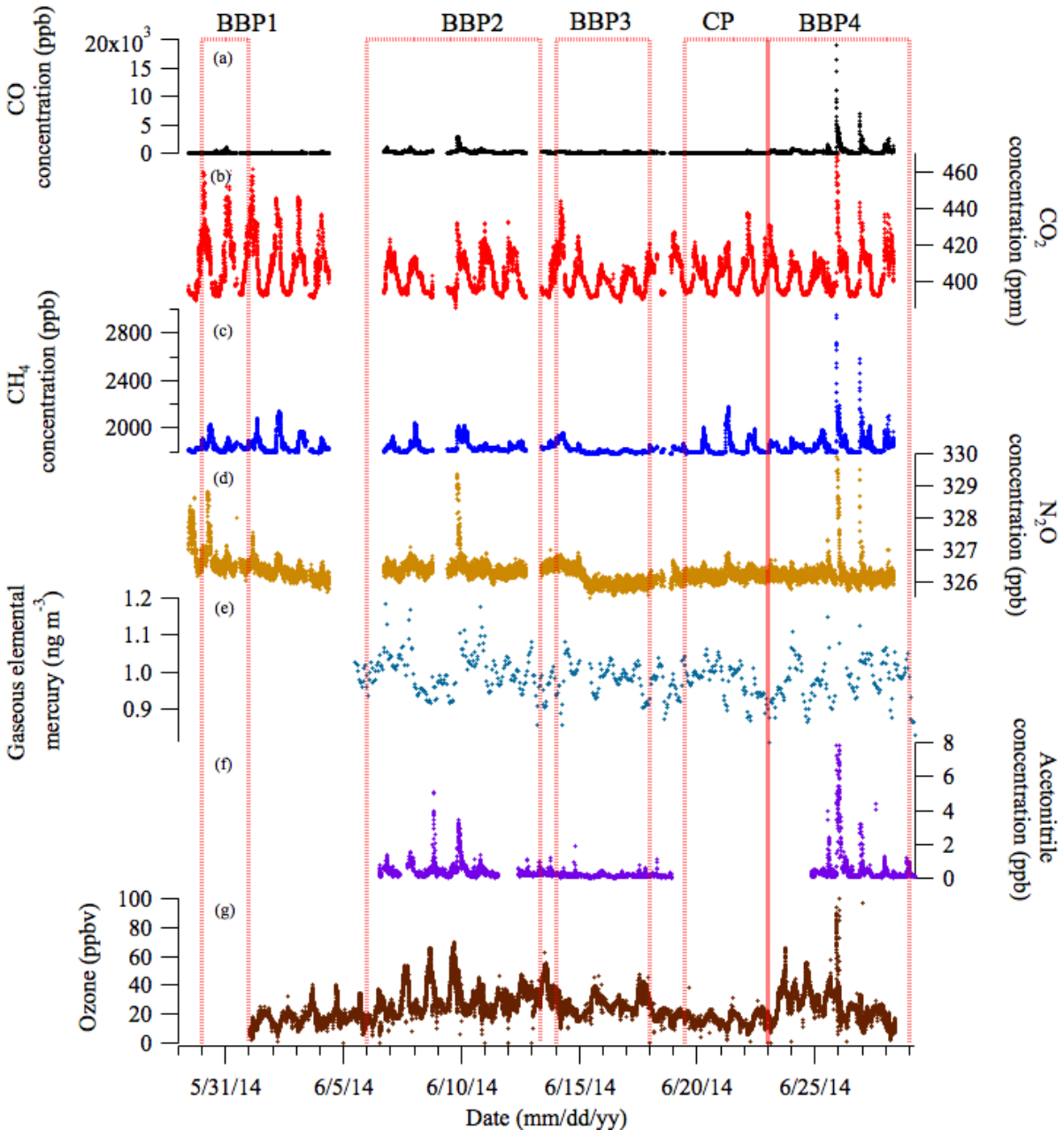

438

439 **Figure 3 The time series of the major measured gaseous species during the SAFIRED campaign: (a) carbon**
440 **monoxide, (b) carbon dioxide, (c) methane, (d) nitrous oxide, (e) gaseous elemental mercury, (f) acetonitrile**
441 **and (g) ozone. The biomass burning and coastal periods are indicated by the red dotted lines. All parts-per**
442 **notation refer to mole fractions unless otherwise indicated. The date and time is local time.**

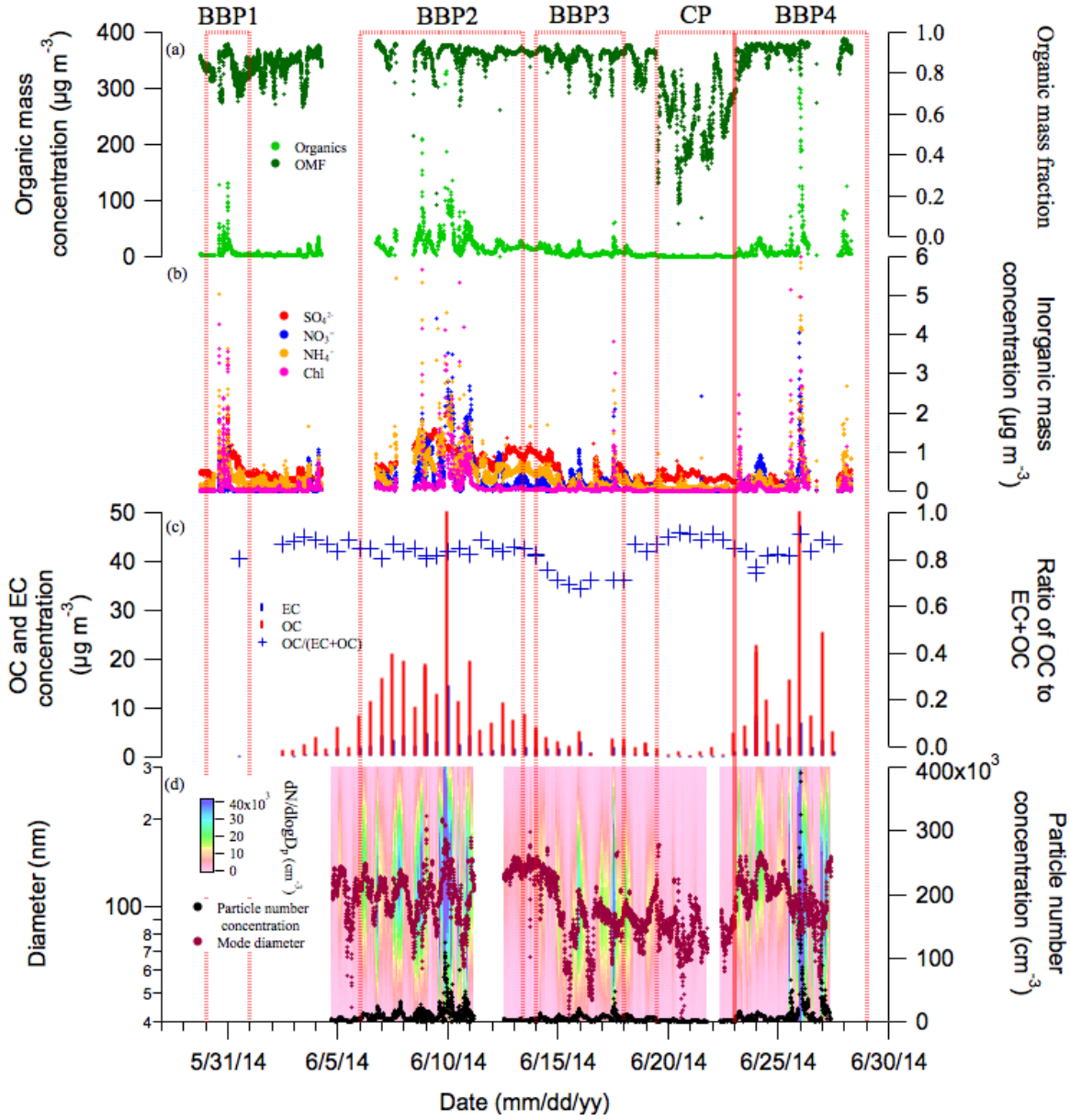

443

444 **Figure 4 The times series of the major aerosol properties during the SAFIRED campaign: (a) the non-**
445 **refractory PM_1 organic mass concentration (left) and organic mass fraction (right), b) the inorganic non-**
446 **refractory PM_1 mass concentrations, (c) the 12-hour filter OC and EC PM_1 mass concentrations (left) and the**
447 **ratio of OC to OC+EC (right), (d) the particle size distributions and particle size mode (left) and the total**
448 **particle number concentration (right) and (e) the wind direction at ATARS. The date and time is local time.**

449 Most of the gaseous and aerosol time series show a pronounced diurnal trend, with
450 higher concentrations typically observed during the night (see Supplementary Figures
451 S2 and S3). This is likely due to a combination of variations in fire locations, time of
452 burns, and changes in the boundary layer height or wind velocity. The diurnals trends
453 of radon concentrations, temperature, wind speed and wind direction for each of the
454 BBPs and the CP are displayed in Figure 5. The radon concentrations provide further

information regarding the regional air mass origins and the degree of contact with the land surface and give insight into the boundary layer. Sharp decreases in the radon concentrations were observed after 09:00 local time and did not increase until after sunset at approximately 18:00 for all periods (Figure 5a), suggesting a pronounced diurnal variation in the boundary layer height. Furthermore, radon concentrations were consistently lower during the CP than the BB periods, suggesting less terrestrial influence than the rest of the sampling period. The HYSPLIT air mass back trajectory for the CP originated along the east coast of Australia and passing over little land before arriving at the station. Figure 5d supports this, showing predominately easterly and northeasterly winds during the night and day, respectively. The diurnal variations during the BB periods were more pronounced. The winds during these periods were predominately southeasterly during the night and morning, turning easterly during the afternoon before reverting at approximately 20:00 local time. The HYSPLIT air mass back trajectories for the BB periods indicated terrestrial origins, with air masses passing predominately over the savannah region of northern Australia where the fires occurred.

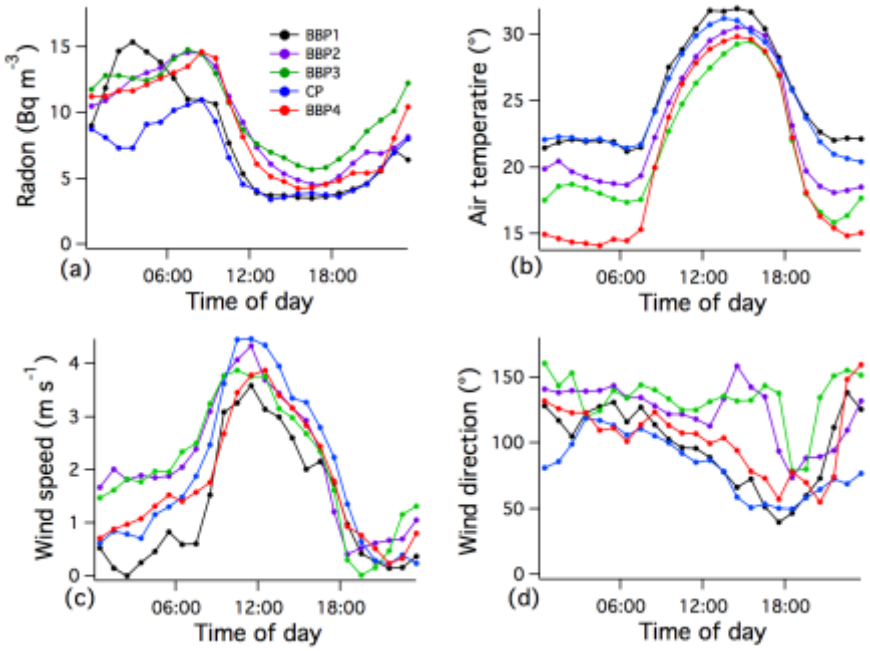

Figure 5 Mean hourly diurnal (a) radon, (b) wind speed, (c) wind direction, and (d) dew point temperature at ATARS, separated into different biomass burning periods (BBP) and a coastal period (CP).

With numerous fires occurring across the region and the limitations of once-per-day satellite fly-overs and stationary measurements, it can be difficult to identify the exact source of these elevated signals. Nonetheless, it is possible to link detected plumes with fires given back trajectory analysis. The elevated signals during BBP1 were likely a result of several fires that were burning and observed on the 30th of May at 14:00 local time approximately 2 and 10 km from ATARS during the day. While the elevated signals were observed later in the evening, it is likely that they were due to a continuation or evolution of those fires. Some of the most intense signals of the campaign were observed during BBP2, with numerous close (within 50 km) and distant (within 200 km) detected. Due to the limitations of the once-per-day satellite fly-by, it was only possible to link one of the observed plumes to a source during this period. A large event observed on the evening of the 9th of June was likely due to a cluster of fires detected approximately 5 km southeast of ATARS. Only one fire within 20 km of ATARS was observed via satellite during BBP3 on the 17th of June but this was not

associated with any significant increase in gaseous or aerosol concentrations. Several fires were also observed between 20 km and 50 km from the station. One close fire was also observed during CP, however wind directions during this period were typically north-easterly and concentrations were therefore much lower. 5-day HYSPLIT trajectories also show that air mass during the CP originated along the east coast of Australia before travelling towards the sampling station with very little terrestrial influence.

For a portion of BBP4, fires were burning within several kilometers of ATARS and several plumes were easily observed from the station. The signals from these plumes are shown in Figure 6. The observed enhancements between 12:30 and 15:00 pm on the 25th June during BBP4 were a result of grass fires burning approximately 2 km south-east from the station. During this event, the wind direction was highly variable, changing between 140° and 80° True Bearing (TB) multiple times. As a result, the sampling changed from measuring the air mass with and without the plume from this fire, which led to sharp increases and decreases in biomass burning-related signals. Visually, the fire area and extent of the plume was larger at 4:00pm than earlier, however the wind direction changed to north-easterly which directed the plume away from the station. From 16:00 until 22:00, the wind direction was stable at approximately 50° TB. At 22:00, the wind direction rapidly changed to directly south and the largest enhancements for the whole campaign were observed until approximately 2:00 am on the 26th of June. It is very likely that these signals were a result of a continuation and evolution of these fires as the night progressed. Portions of a ~0.25 km^2 grassland field within 500 m directly south of ATARS were observed to be burned upon arrival at the station on the morning of the 26th of June and we speculate

that the burning of this field contributed to the large enhancements in measured biomass burning emissions. The emissions during this portion of BBP4 are likely to be the most representative of fresh biomass burning smoke during the SAFIRED campaign. Significant ozone enhancements over 80 ppb were observed during this event, although this was likely result of a cross-contamination due to concurrently high concentrations of UV-absorbing organic compounds in the gaseous phase. This enhancement would only be possible with significant photochemical processing which is very unlikely considering the time of the event, the visual evidence of close fires, and the large concentrations observed.

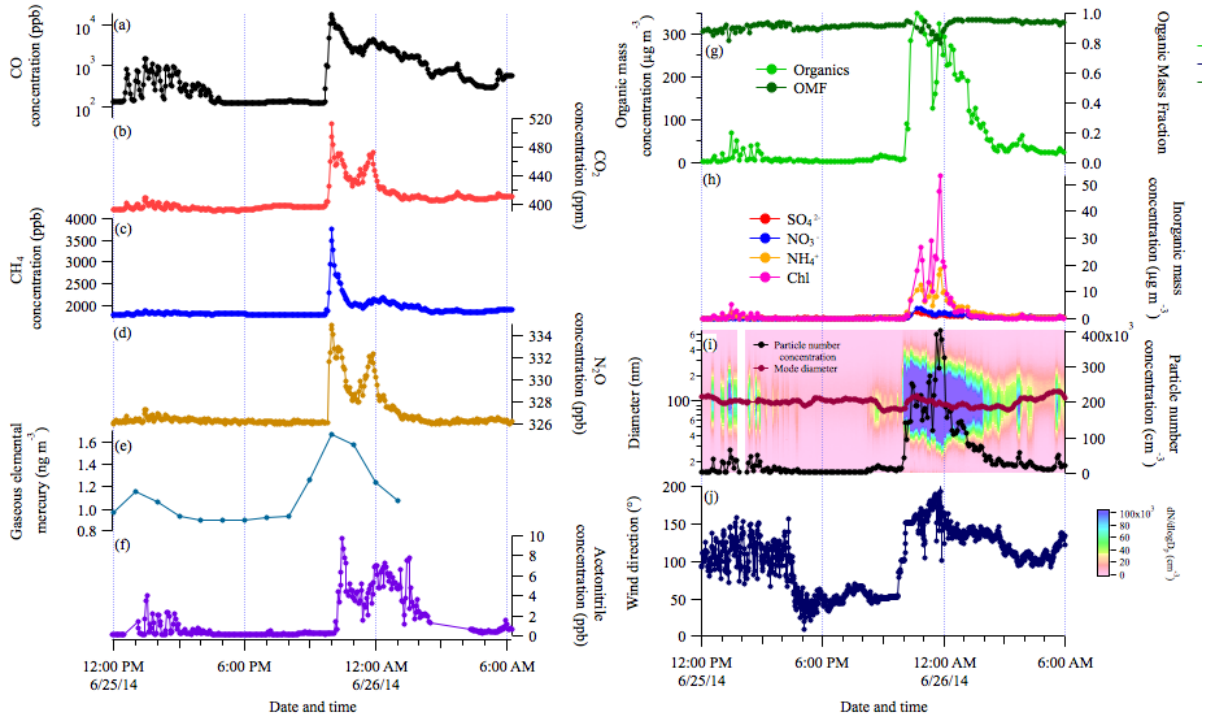

Figure 6 The major gas and aerosol concentrations measured during two biomass burning events within 1 km of ATARS during BBP4. (a) through (g) and (h) through (k) are as per Figures 3 and 4, respectively. All parts-per notation or mole fractions unless otherwise indicated. The date and time are local time.

Based on the elevated concentrations of biomass burning related gaseous and aerosol species, detection of close fires and the air mass back trajectory analysis during portions of BBP1, BBP2 and BBP4, these periods are likely associated with fresh biomass burning smoke from nearby fires. With smaller concentrations and more distant

observed fires, the signals observed during BBP3 are possibly more characteristic of aged biomass burning smoke. The influence of biomass burning during CP was much smaller than the rest of the campaign. Investigating the relationship between toluene and acetonitrile, two NMOCs emitted from biomass burning, can provide further information on the aging of BB emissions. Toluene is much shorter lived than acetonitrile as it readily reacts in the presence of the OH radical. Assuming a consistent emission ratio of these two NMOCs from fires in this region, the ratio of toluene/acetonitrile thereby provides a proxy for photochemical age. Unfortunately, the PTR-MS which measures these species was not operational during BBP1 and CP. The diurnal trends for the toluene and acetonitrile concentrations and the toluene/acetonitrile ratio is shown in Figure 7 for BBP2, BBP3 and BBP4. The toluene/acetonitrile ratio was highest during the night, indicating more photochemically aged smoke throughout the day. Interestingly, while the toluene and acetonitrile concentrations were consistently higher during BBP2 and BBP4 than BBP3, the toluene/acetonitrile ratio was of the same magnitude and followed the same trend. It is therefore plausible that, while there were not large enhancements in concentrations during BBP3 and there were few fires detected close-by during the daytime satellite flyovers, there were small-scale burns during the night that were close enough for the emissions to reach sampling site. This observation highlights the limitation of using satellite hotspot detection in fully understanding the aging processes of biomass burning emissions.

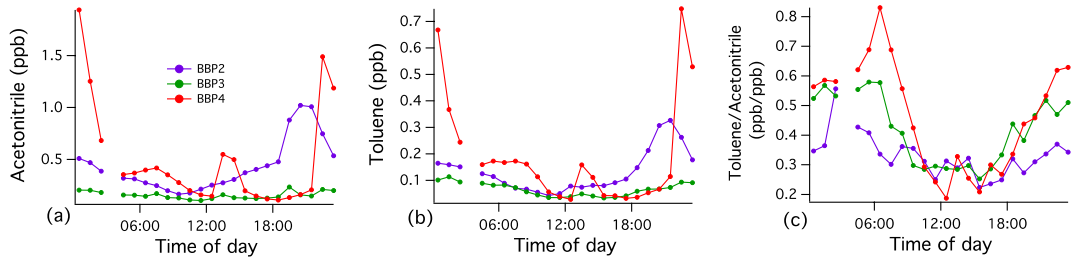

Figure 7 Mean hourly diurnal (a) acetonitrile concentration, (b) toluene concentration, (c) toluene/acetonitrile ratio, separated into different biomass burning periods (BBP).

Particle size distributions were unimodal for the majority of the sampling period with a mode of approximately 100 nm on average (see Figure 8). The SMPS was not operational during BBP1. Although the shape of the BBP4 size distribution was similar to the campaign average, concentrations were much higher and a result of close fires. BBP2 had a slightly larger size distribution centered on 110 nm. The size distribution during BBP3 was slightly smaller than the campaign average and BBP2 and BBP4, with a mode centered on ~95 nm. Furthermore, the diurnal trends of the BBA mode diameter during BBP2, BBP3 and BBP4 and CP all showed a clear maximum during the night (see Supplementary Figure S3d). The diurnal trends of the toluene/acetonitrile ratios (Figure 7c) as well as the ratio of oxygenated organic aerosol to total organics (see Supplementary Figure S3c) suggest that the larger night time particle sizes are more associated with fresh biomass burning. The contrast between these size distributions could be a result of atmospheric aging and dilution in which organic mass condenses onto or evaporates from the particle. Variations in fuel load or burning conditions could also contribute to this difference. The size and concentration of particles during the Coastal Period (CP) were much smaller than the rest of the campaign. There were two periods during CP where a bimodal size distribution was observed; one from approximately 3 pm until midnight on the 19th of June and the other between 2 pm and 6 pm on the 20th of June. The size distributions for both of these

periods had a mode at approximately 20 nm and another at approximately 85 nm. Submicron sulfates made up to 32% of the total submicron non-refractory mass concentrations, as reported by the cToF-AMS from the period of midday on the 19th of June until midnight on the 22nd of June, whereas the average sulfate contribution for the rest of the campaign was approximately 8%. The low radon values, small particle concentrations, bimodal size distributions and significant contributions of sulfate during this period also suggest very little biomass burning signal and a more marine-like aerosol. No particle nucleation events were observed over the entire sampling period (See Supplementary Figure S4). This is likely due to the elevated particle concentrations acting as a condensation sink.

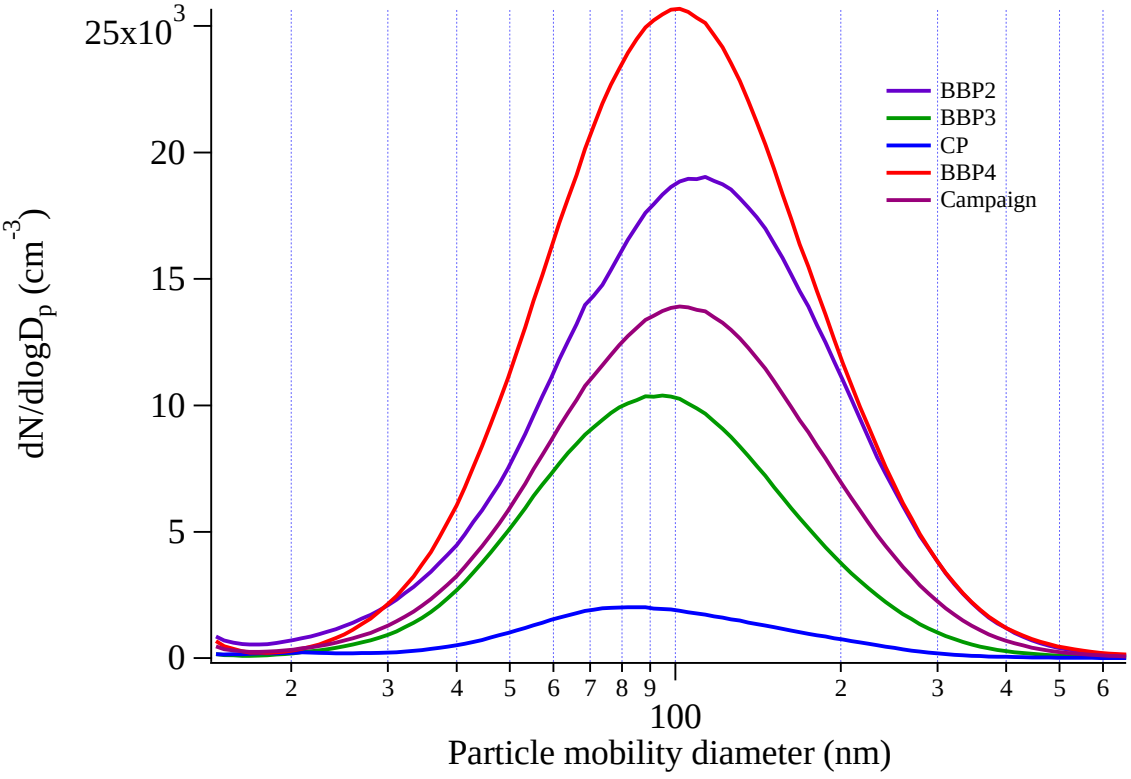

Figure 8 The average number size distribution during BBP2, BBP3, BBP4, CP and the campaign average.

Over the campaign, organics dominated the non-refectory sub-micron aerosol mass contributing, on average, 90% of the total mass. Sulphate, nitrates, ammonium and

chloride species contributed the rest of this mass, with the largest contributions from sulphate and ammonium. Sulphate contributions were very significant during the coastal period, contributing up to 32% of the total mass. Although chlorides contributed the least to the total mass on average, during clear biomass burning events where sharp increases in CO and organics were observed, chlorides made up the largest component of inorganic aerosol. Organic carbon made up approximately 80% to 90% of the total carbon (organic carbon + elemental carbon) PM_1 mass during the campaign, with the exception of BBP3, when this dropped to 70%. Whether these observations were a result of burn conditions or aging processes (i.e. evaporation of organic compounds from the aerosol phase) is unclear.

4. Outcomes of SAFIRED

The overall aim of this study was to investigate the characteristics of BB emissions in the tropical savannah region of northern Australia during the early dry season. For many gaseous and aerosol species, elevated signals were observed for much of the month-long sampling period due to the high frequency of fires. Further analysis of these species can provide more insight into the impact of these fires on the regional atmosphere. Table 2 displays a summary of companion studies undertaken within the SAFIRED campaign.

Table 3 A list of currently published companion studies undertaken during SAFIRED.

Reference	Title
Winton et al., (2016)	Dry season aerosol iron solubility in tropical northern Australia

Wang et al., (2017)	Emissions of selected semivolatile organic chemicals from forest and savannah fires
Milic et al., (2017)	Biomass burning and biogenic aerosols in northern Australia during the SAFIRED campaign
Mallet et al., (2017)	Composition, size and cloud condensation nuclei activity of biomass burning aerosol from northern Australian savannah fires
Desservattaz et al., (2017)	Emission factors of trace gases and particles from tropical savanna fires in Australia
Howard et al., (2017)	Atmospheric mercury in the southern hemisphere tropics: seasonal and diurnal variations and influence of inter-hemispheric transport

611

612 **4.1. Emission factors and gaseous species loadings**

613 Desservattaz et al., (under review) identified individual plumes with high signals during
614 SAFIRED in order to determine emissions factors CO_2, CO, CH_4. N_2O, as well as GEM,
615 Aitken and Accumulation mode aerosols and submicron non-refractory particle species
616 (organics, sulfates, nitrates, ammonium and chlorides). Seasonal emission factors for
617 the major greenhouse gases are important for national greenhouse gas inventories and
618 in understanding the impact of savannah fires. Furthermore, these results will be the
619 first set of emission factors for aerosol particles from savannah fires in Australia, with
620 early results suggesting higher factors than those observed from African and South
621 American savannah fires. Emission factors were mostly found to be dependent on the
622 combustion conditions (using the modified combustion efficiency as a proxy) of the
623 fires.

Wang et al. (2017) investigated 13 major PAH compounds in both the gaseous and aerosol phase during the SAFIRED campaign and estimated their emission factors from savannah fires, as well as for subtropical eucalypt forest fires. Concentrations of these PAHs varied from from ~ 1 to over 15 ng m^{-3} within different BB periods and the emission factor for savannah fires for $\sum_{13}$ PAHs were estimated to be 1600 ± 110 µg kg^{-1} In the gas phase, 3- and 4-ring compounds typically contributed ~ 90% to the sum concentrations whereas the particle-associated PAHs were dominated by 5- and 6-ring compounds (> 80%). Measured PAH concentrations were significantly higher during BBP2 and BBP4. During these periods, concentrations of BaP exceeded the monitoring investigation level for atmospheric BaP (0.30 ng m^{-3}) in Australia (National-Environment-Protection-Council-Service-Corporation, 2011) by up to 200%.

Biomass burning produces significant amounts of semi-volatile NMOC which can be difficult to quantify and identify with current measurement techniques. However recent studies have shown that including semi volatile NMOC chemistry in models improves the agreement between the modeled and observed organic aerosol (Alvarado et al., 2015; Konovalov et al., 2015) and ozone (Alvarado et al., 2015). High quality NMOC emission factors are crucial for models to assess the impact of biomass burning plumes on air quality and climate. Future analyses will be undertaken on the SAFIRED data to quantify emission factors for various NMOCs.

SAFIRED represents the first measurements of atmospheric mercury undertaken in the tropical region of the Australian continent. The mean observed GEM concentration over the study period was 0.99 ± 0.09 ng m^{-3}, similar to the average over that month

649 (0.96 ng m^{-3}) for 5 other Southern Hemisphere sites and slightly lower than the average
650 (1.15 ng m^{-3}) for 5 tropical sites (Sprovieri et al., 2016). Mean GOM and PBM
651 concentrations were 11 ± 5 pg m^{-3} and 6 ± 3 pg m^{-3} respectively, representing 0.6 –
652 3.4% of total observed atmospheric mercury. During periods of pronounced trace gas
653 and aerosol concentrations during the campaign, spikes in GEM concentrations were
654 also observed, though there were no significant increases in GOM or PBM. Emission
655 ratios calculated during the campaign were two orders of magnitude higher than those
656 reported by Andreae and Merlet (2001). Future outcomes from the SAFIRED campaign
657 will focus on the use of micrometeorological techniques and the passive tracer radon to
658 quantify delivery of atmospheric mercury to tropical savannah ecosystems. ATARS
659 also now serves as an additional site measuring continuous GEM as part of the Global
660 Mercury Observation System (GMOS), one of only two tropical observing sites in the
661 Eastern Hemisphere and the third such site located in Australia. A discussion of the
662 seasonal and diurnal variations of atmospheric mercury at the ATARS site can be found
663 in Howard et al. (2017).

664 **4.2. Biomass burning aerosol chemistry**

665 Milic et al., (2017) provided further analysis into the aerosol chemical composition to
666 elucidate the aging of early dry season biomass burning emissions. Fractional analysis
667 (e.g., f44 and f60, the fraction of m/z 44 and m/z 60 to all organic masses, indicated
668 oxygenation and BB sources, respectively) and factor analysis using positive matrix
669 factorisation (PMF) of cToF-AMS data was investigated over the entire sampling
670 period. Outside of the periods of significant influence from BB events, three PMF-
671 resolved organic aerosol factors were identified. A BB organic aerosol factor was found
672 to comprise 24% of the submicron non-refractory organic mass, with an oxygenated
673 organic aerosol factor and a biogenic isoprene-related secondary organic aerosol factor

674 comprising 47% and 29%, respectively. These results indicate the significant influence
675 of fresh and aged BB on aerosol composition in the early dry season. The emission of
676 precursors from fires is likely responsible for some of the SOA formation.
677
678 The water uptake of aerosols during SAFIRED was further investigated in Mallet et al.,
679 (2017) to identify the influence of early dry season BB in this region on cloud
680 formation. The concentrations of cloud condensation nuclei at a constant
681 supersaturation of 0.5% were typically of the order of 2000 cm^{-3} and reached well over
682 10000 cm^{-3} during intense BB events. Variations in the ratio of aerosol particles
683 activating cloud droplets showed a distinct diurnal trend, with an activation ratio of
684 40% ± 20% during the night and 60% ± 20% during the day. The particle size
685 distribution and the hygroscopicity of the particles were found to significantly influence
686 this activation ratio. Particles were generally extremely hydrophobic, particularly
687 during the night and during the BB periods shown in this paper. Modelling CCN
688 concentrations using the size distributions of aerosols and typical continental and
689 terrestrial values of hygroscopicities yielded significant over predictions of up more
690 than 200%, highlighting the need to include more regional parameterisations of aerosol
691 composition and hygroscopicity.
692
693 Furthermore the fractional solubility of aerosol iron and other trace metals during
694 SAFIRED were investigated in Winton et al., (2016). The fractional iron solubility is
695 an important variable determining iron availability for biological uptake in the ocean.
696 On a global scale, the large variability in the observed fractional iron solubility results,
697 in part, from a mixture of different aerosol sources. Estimates of fractional iron
698 solubility from fire combustion (1 - 60 %) are thought to be greater than those

originating from mineral dust (1 - 2%) (Chuang et al., 2005;Guieu et al., 2005;Sedwick et al., 2007), and may vary in relationship to biomass and fire characteristics as well as that of the underlying terrain (Paris et al., 2010;Ito, 2011). Iron associated with BB may provide information with respect to BB inputs of iron to the ocean (Giglio et al., 2013;e.g. Meyer et al., 2008). The ATARS provides an ideal location to further investigate BB derived fractional iron solubility at the source. The results from this study can be found in Winton et al. (2016) and show that soluble iron concentrations from BB sources are significantly higher than those observed in Southern Ocean baseline air masses from the Cape Grim Baseline Air Pollution Station, Tasmania, Australia (Winton et al., 2015). Aerosol iron at SAFIRED was a mixture of fresh BB, mineral dust, sea spray and industrial pollution sources. The fractional iron solubility (2 - 12%) was relatively high throughout the campaign and the variability was related to the mixing and enhancement of mineral dust iron solubility with BB species.

5. Conclusions and looking forward

Biomass burning was found to significantly influence the surface atmospheric composition during the 2014 early dry season in north Australia. Over 28000 fires were detected via satellite retrieval during the sampling period. Several periods were identified when fires within 20 km of the research station resulted in significant enhancements of greenhouse gases, non-methane gaseous organic compounds, gaseous elemental mercury and polycyclic aromatic hydrocarbons and aerosol loadings. Much of the PM_1 mass was comprised of organic material. The aerosol particle number size distributions were typically unimodal and centered around 100 nm which is smaller than BBA observed in other regions. The analysis of the time series of these measured quantities has so far allowed the quantification of savannah fire emission factors for

these aerosol and gaseous species and has provided and understanding of the aerosol aging, water uptake and solubility in this region.

While the specific outcomes of the SAFIRED campaign are reviewed in the previous section, the general importance of this study can be discussed in a greater context. This is the first large-scale collaborative project undertaken in this region and draws on the resources and expertise of most of Australia's research institutes focused on atmosphere chemistry and composition. Large scale, multidisciplinary measurement campaigns in the tropics, such as SAFIRED, are needed to make distinctions between different types of fires in different regions to reduce uncertainties in global climate models (Keywood et al., 2013). This need has been recognized with the formation of global collaborative initiatives promoting interdisciplinary collaboration in biomass burning research (Kaiser and Keywood, 2015). As the world moves towards a warmer climate, it is plausible that the frequency and intensity of biomass burning will increase, and these emissions will become an increasingly important source of trace gases and aerosols to the atmosphere.

SAFIRED lays the foundation for future measurements at ATARS that could make measurements throughout the whole dry season and on a more long-term scale. Future work in this region should focus on 1) the detailed characterisation of individual fires and their emissions, 2) biomass burning emissions throughout the late dry season and 3) the vertical and horizontal transport of biomass burning emissions in this region. With well-established emission factors, a concentrated effort should be made to link modelled aerosol gaseous and aerosol loadings with *in situ* and remote sensing measurements. This should be done not just at the surface, but throughout the boundary

748 layer as well as over the waters north of Australia. Furthermore, a further investigation
749 of the radiative influence of the gaseous and aerosol species should be done for this
750 region.

751 Data availability

752 All data are available upon request from the corresponding authors (Branka Miljevic,
753 b.miljevic@qut.edu.au; Melita D. Keywood; melita.keywood@csiro.au).

754 Author Contributions

755 M.D. Mallet[a,b,c,d,e], M.J. Desservettaz[b,c,d,e], B. Miljevic[b,c,e*], A. Milic[b,d,e], Z.D.
756 Ristovski[b,e], J. Alroe[b,c,e], L.T. Cravigan[b,c,e], E.R. Jayaratne[d,e], C. Paton-Walsh[b,c,e],
757 D.W.T. Griffith[b,d,e], S.R. Wilson[b,d,e], G. Kettlewell[b,e], M.V. van der Schoot[b,e], P.
758 Selleck[b,c,d,e], F. Reisen[b,c,e], S.J. Lawson[b,c,d,e], J. Ward[b,c,d,e], J. Harnwell[b,c,e], M.
759 Cheng[b,c,d,e], R.W. Gillett[b,c,d,e], S.B. Molloy[d,e], D. Howard[b,c,d,e], P.F. Nelson[b,e], A.L
760 Morrison[b,e], G.C. Edwards[b,c,e], A.G. Williams[b,c,e], S.D. Chambers[b,c,d,e], S.
761 Werczynski[b,c,e], L.R. Williams[c,d,e], V.H.L. Winton[b,c,d,e], and B. Atkinson[b,c], X.
762 Wang[b,d,e], M.D. Keywood[b,c,d,e,f*]

763 a: Wrote and organised the manuscript
764 b: Contributed to the organisation of the campaign
765 c: Installed and/or operated instrumentation during the sampling period
766 d: Analysed data
767 e: Contributed to the manuscript and/or data interpretation
768 f: Designed and led the campaign.
769 *: Corresponding author

Competing interests

The authors declare that they have no conflict of interest.

Acknowledgements

The majority of the campaign was internally funded. The input of QUT was supported by the Australian Research Council Discovery (Grant DP120100126). The work on aerosol iron solubility was supported by Curtin University (RES-SE-DAP_AW-47679-1), the University of Tasmania (B0019024) and the Australian Research Council (Grant FT130100037).

6. References

Akagi, S. K., Craven, J. S., Taylor, J. W., McMeeking, G. R., Yokelson, R. J., Burling, I. R., Urbanski, S. P., Wold, C. E., Seinfeld, J. H., Coe, H., Alvarado, M. J., and Weise, D. R.: Evolution of trace gases and particles emitted by a chaparral fire in California, Atmospheric Chemistry and Physics, 12, 1397-1421, 2012.

Andersen, A. N., Cook, G. D., Corbett, L. K., Douglas, M. M., Eager, R. W., Russell-Smith, J., Setterfield, S. A., Williams, R. J., and Woinarski, J. C.: Fire frequency and biodiversity conservation in Australian tropical savannas: implications from the Kapalga fire experiment, Austral Ecology, 30, 155-167, 2005.

Bindoff, N. L., Stott, P. A., AchutaRao, K. M., Allen, M. R., Gillett, N., Gutzler, D., Hansingo, K., Hegerl, G., Hu, Y., Jain, S., Mokhov, I. I., Overland, J., Perlwitz, J., Sebbari, R., and Zhang, X.: Detection and Attribution of Climate Change: from Global to Regional, in: Climate Change 2013: The Physical Science Basis. Contribution of Working Group I to the Fifth Assessment Report of the Intergovernmental Panel on Climate Change, edited by: Stocker, T. F., Qin, D., Plattner, G.-K., Tignor, M., Allen, S. K., Boschung, J., Nauels, A., Xia, Y., Bex, V., and Midgley, P. M., Cambridge University Press, Cambridge, United Kingdom and New York, NY, USA, 867–952, 2013.

Chambers, S. D., Hong, S.-B., Williams, A. G., Crawford, J., Griffiths, A. D., and Park, S.-J.: Characterising terrestrial influences on Antarctic air masses using Radon-222 measurements at King George Island, Atmospheric Chemistry and Physics, 14, 9903-9916, 2014.

Chow, J. C., Watson, J. G., Chen, L. W. A., Chang, M. C. O., Robinson, N. F., Trimble, D., and Kohl, S.: The IMPROVE-A temperature protocol for thermal/optical carbon analysis: maintaining consistency with a long-term database, Journal of the Air & Waste Management Association, 57, 1014-1023, 2007a.

804 Chow, J. C., Watson, J. G., Chen, L. W. A., Chang, M. O., Robinson, N. F., Trimble,
805 D., and Kohl, S.: The IMPROVE-A temperature protocol for thermal/optical carbon
806 analysis: maintaining consistency with a long-term database, Journal of the Air &
807 Waste Management Association, 57, 1014-1023, 2007b.
808 Chuang, P. Y., Duvall, R. M., Shafer, M. M., and Schauer, J. J.: The origin of water
809 soluble particulate iron in the Asian atmospheric outflow, Geophysical Research
810 Letters, 32, L07813, 2005.
811 Crutzen, P. J., and Andreae, M. O.: Biomass burning in the tropics: Impact on
812 atmospheric chemistry and biogeochemical cycles, Science, 250, 1669-1678, 1990.
813 Draxler, R. R., and Rolph, G.: HYSPLIT (HYbrid Single-Particle Lagrangian
814 Integrated Trajectory) model access via NOAA ARL READY website (http://www/.
815 arl. noaa. gov/ready/hysplit4. html). NOAA Air Resources Laboratory, Silver Spring,
816 in, Md, 2003.
817 Du, H., Kong, L., Cheng, T., Chen, J., Du, J., Li, L., Xia, X., Leng, C., and Huang, G.:
818 Insights into summertime haze pollution events over Shanghai based on online water-
819 soluble ionic composition of aerosols, Atmospheric Environment, 45, 5131-5137, 2011.
820 Edwards, G. C., Rasmussen, P. E., Schroeder, W. H., Wallace, D. M., Halfpenny-
821 Mitchell, L., Dias, G. M., Kemp, R. J., and Ausma, S.: Development and evaluation of
822 a sampling system to determine gaseous Mercury fluxes using an aerodynamic
823 micrometeorological gradient method, Journal of Geophysical Research: Atmospheres,
824 110, 2005.
825 Ferek, R. J., Reid, J. S., Hobbs, P. V., Blake, D. R., and Liousse, C.: Emission factors
826 of hydrocarbons, halocarbons, trace gases and particles from biomass burning in Brazil,
827 Journal of Geophysical Research, 103, 107-132, 1998.
828 Giglio, L., Randerson, J. T., and Werf, G. R.: Analysis of daily, monthly, and annual
829 burned area using the fourth-generation global fire emissions database (GFED4),
830 Journal of Geophysical Research: Biogeosciences, 118, 317-328, 2013.
831 Govender, N., Trollope, W. S., and Van Wilgen, B. W.: The effect of fire season, fire
832 frequency, rainfall and management on fire intensity in savanna vegetation in South
833 Africa, Journal of Applied Ecology, 43, 748-758, 2006.
834 Griffith, D. W. T.: Synthetic calibration and quantitative analysis of gas-phase FT-IR
835 spectra, Applied Spectroscopy, 50, 59-70, 1996.
836 Griffith, D. W. T., Deutscher, N. M., Caldow, C., Kettlewell, G., Riggenbach, M., and
837 Hammer, S.: A Fourier transform infrared trace gas and isotope analyser for
838 atmospheric applications, Atmos. Meas. Tech., 5, 2481-2498, 2012.
839 Guieu, C., Bonnet, S., Wagener, T., and Loÿe-Pilot, M. D.: Biomass burning as a source
840 of dissolved iron to the open ocean?, Geophysical Research Letters, 32, 2005.
841 Gustin, M. S., Lindberg, S. E., and Weisberg, P. J.: An update on the natural sources
842 and sinks of atmospheric mercury, Applied Geochemistry, 23, 482-493, 2008.
843 Honninger, G., von Friedeburg, C., and Platt, U.: Multi axis differential optical
844 absorption spectroscopy (MAX-DOAS), Atmospheric Chemistry and Physics, 4, 231-
845 254, 2004.
846 Howard, D., Nelson, P. F., Edwards, G. C., Morrison, A. L., Fisher, J. A., Ward, J.,
847 Harnwell, J., van der Schoot, M., Atkinson, B., Chambers, S. D., Griffiths, A. D.,
848 Werczynski, S., and Williams, A. G.: Atmospheric mercury in the southern hemisphere
849 tropics: seasonal and diurnal variations and influence of inter-hemispheric transport,
850 Atmos. Chem. Phys. Discuss., 2017, 1-20, 10.5194/acp-2017-307, 2017.
851 Iinuma, Y., Engling, G., Puxbaum, H., and Herrmann, H.: A highly resolved anion-
852 exchange chromatographic method for determination of saccharidic tracers for biomass

853 combustion and primary bio-particles in atmospheric aerosol, Atmospheric
854 Environment, 43, 1367-1371, 2009.
855 Ito, A.: Mega fire emissions in Siberia: potential supply of bioavailable iron from
856 forests to the ocean, Biogeosciences, 8, 1679-1697, 2011.
857 Jacobson, M. Z.: Strong radiative heating due to the mixing state of black carbon in
858 atmospheric aerosols, Nature, 409, 695-697, 2001.
859 Kaiser, J. W., and Keywood, M.: Preface for Atmos. Env. Special issue on IBBI,
860 Atmospheric Environment, 121, 1-3, 2015.
861 Keil, A., and Haywood, J. M.: Solar radiative forcing by biomass burning aerosol
862 particles during SAFARI 2000: A case study based on measured aerosol and cloud
863 properties, Journal of Geophysical Research: Atmospheres, 108, 2003.
864 Keywood, M., Kanakidou, M., Stohl, A., Dentener, F., Grassi, G., Meyer, C. P.,
865 Torseth, K., Edwards, D., Thompson, A. M., Lohmann, U., and Burrows, J.: Fire in the
866 air: Biomass burning impacts in a changing climate, Critical Reviews in Environmental
867 Science and Technology, 43, 40-83, 2013.
868 Landis, M. S., Stevens, R. K., Schaedlich, F., and Prestbo, E. M.: Development and
869 characterization of an annular denuder methodology for the measurement of divalent
870 inorganic reactive gaseous mercury in ambient air, Environmental science &
871 technology, 36, 3000-3009, 2002.
872 LaRoche, J., and Breitbarth, E.: Importance of the diazotrophs as a source of new
873 nitrogen in the ocean, Journal of Sea Research, 53, 67-91, 2005.
874 Lawson, S. J., Keywood, M. D., Galbally, I. E., Gras, J. L., Cainey, J. M., Cope, M. E.,
875 Krummel, P. B., Fraser, P. J., Steele, L. P., Bentley, S. T., Meyer, C. P., Ristovski, Z.,
876 and Goldstein, A. H.: Biomass burning emissions of trace gases and particles in marine
877 air at Cape Grim, Tasmania, Atmospheric Chemistry and Physics, 15, 13393-13411,
878 2015.
879 Lin, N.-H., Tsay, S.-C., Maring, H. B., Yen, M.-C., Sheu, G.-R., Wang, S.-H., Chi, K.
880 H., Chuang, M.-T., Ou-Yang, C.-F., and Fu, J. S.: An overview of regional experiments
881 on biomass burning aerosols and related pollutants in Southeast Asia: From BASE-
882 ASIA and the Dongsha Experiment to 7-SEAS, Atmospheric Environment, 78, 1-19,
883 2013.
884 Liousse, C., Devaux, C., Dulac, F., and Cachier, H.: Aging of savanna biomass burning
885 aerosols: Consequences on their optical properties, Journal of Atmospheric Chemistry,
886 22, 1-17, 1995.
887 Manninen, H. E., Petaja, T., Asmi, E., Riipinen, I., Nieminen, T., Mikkila, J., Horrak,
888 U., Mirme, A., Mirme, S., Laakso, L., Kerminen, V. M., and Kulmala, M.: Long-term
889 field measurements of charged and neutral clusters using Neutral cluster and Air Ion
890 Spectrometer (NAIS), Boreal Environment Research, 14, 591-605, 2009.
891 Meyer, C., Cook, G., Reisen, F., Smith, T., Tattaris, M., Russell-Smith, J., Maier, S.,
892 Yates, C., and Wooster, M.: Direct measurements of the seasonality of emission factors
893 from savanna fires in northern Australia, Journal of Geophysical Research:
894 Atmospheres (1984–2012), 117, 2012.
895 Meyer, C. P., Luhar, A. K., and Mitchell, R. M.: Biomass burning emissions over
896 northern Australia constrained by aerosol measurements: I—Modelling the distribution
897 of hourly emissions, Atmospheric Environment, 42, 1629-1646, 2008.
898 Mirme, A., Tamm, E., Mordas, G., Vana, M., Uin, J., Mirme, S., Bernotas, T., Laakso,
899 L., Hirsikko, A., and Kulmala, M.: A wide-range multi-channel Air Ion Spectrometer,
900 Boreal Environmental Research, 12, 247-264, 2007.
901 National-Environment-Protection-Council-Service-Corporation: National
902 Environment Protection (Air Toxics) Measure, 2011.

Paris, R., Desboeufs, K., Formenti, P., Nava, S., and Chou, C.: Chemical characterisation of iron in dust and biomass burning aerosols during AMMA-SOP0/DABEX: implication for iron solubility, Atmospheric Chemistry and Physics, 10, 4273-4282, 2010.
Penner, J., Chuang, C., and Grant, K.: Climate forcing by carbonaceous and sulfate aerosols, Climate Dynamics, 14, 839-851, 1998.
Rea, A. W., Lindberg, S. E., Scherbatskoy, T., and Keeler, G. J.: Mercury accumulation in foliage over time in two northern mixed-hardwood forests, Water, Air, and Soil Pollution, 133(1-4), 49-67, 2002.
Russell-Smith, J., Yates, C. P., Whitehead, P. J., Smith, R., Craig, R., Allan, G. E., Thackway, R., Frakes, I., Cridland, S., Meyer, M. C. P., and Gill, M.: Bushfires' down under': patterns and implications of contemporary Australian landscape burning, International Journal of Wildland Fire, 16, 361-377, 2007.
Russell-Smith, J., Cook, G. D., Cooke, P. M., Edwards, A. C., Lendrum, M., Meyer, C., and Whitehead, P. J.: Managing fire regimes in north Australian savannas: applying Aboriginal approaches to contemporary global problems, Frontiers in Ecology and the Environment, 11, e55-e63, 2013.
Saarikoski, S., Sillanpää, M., Sofiev, M., Timonen, H., Saarnio, K., Teinilä, K., Karppinen, A., Kukkonen, J., and Hillamo, R.: Chemical composition of aerosols during a major biomass burning episode over northern Europe in spring 2006: Experimental and modelling assessments, Atmospheric Environment, 41, 3577-3589, 2007.
Sedwick, P. N., Sholkovitz, E. R., and Church, T. M.: Impact of anthropogenic combustion emissions on the fractional solubility of aerosol iron: Evidence from the Sargasso Sea, Geochemistry, Geophysics, Geosystems, 8, 2007.
Shi, Y., Matsunaga, T., Saito, M., Yamaguchi, Y., and Chen, X.: Comparison of global inventories of CO_2 emissions from biomass burning during 2002–2011 derived from multiple satellite products, Environmental Pollution, 206, 479-487, 2015.
Singh, H., Brune, W., Crawford, J., Jacob, D. J., and Russell, P.: Overview of the summer 2004 Intercontinental Chemical Transport Experiment–North America (INTEX-A), Journal of Geophysical Research: Atmospheres, 111, 2006.
Sinreich, R., Friess, U., Wagner, T., and Platt, U.: Multi axis differential optical absorption spectroscopy (MAX-DOAS) of gas and aerosol distributions, Faraday Discuss, 130, 153-164, 2005.
Sprovieri, F., Pirrone, N., Bencardino, M., D'Amore, F., Carbone, F., Cinnirella, S., Mannarino, V., Landis, M., Ebinghaus, R., Weigelt, A., Brunke, E. G., Labuschagne, C., Martin, L., Munthe, J., Wängberg, I., Artaxo, P., Morais, F., Cairns, W., Barbante, C., Diéguez, M. D. C., Garcia, P. E., Dommergue, A., Angot, H., Magand, O., Skov, H., Horvat, M., Kotnik, J., Read, K. A., Neves, L. M., Gawlik, B. M., Sena, F., Mashyanov, N., Obolkin, V. A., Wip, D., Feng, X. B., Zhang, H., Fu, X., Ramachandran, R., Cossa, D., Knoery, J., Marusczak, N., Nerentorp, M., and Norstrom, C.: Atmospheric Mercury Concentrations observed at ground-based monitoring sites globally distributed in the framework of the GMOS network, Atmospheric Chemistry and Physics Discussions, 2016, 1-32, 2016.
Steffen, A., Douglas, T., Amyot, M., Ariya, P., Aspmo, K., Berg, T., Bottenheim, J., Brooks, S., Cobbett, F., Dastoor, A., Dommergue, A., Ebinghaus, R., Ferrari, C., Gardfeldt, K., Goodsite, M. E., Lean, D., Poulain, A. J., Scherz, C., Skov, H., Sommar, J., and Temme, C.: A synthesis of atmospheric mercury depletion event chemistry in the atmosphere and snow, Atmospheric Chemistry and Physics, 8, 1445-1482, 2008.

Stockwell, C., Yokelson, R., Kreidenweis, S., Robinson, A., DeMott, P., Sullivan, R., Reardon, J., Ryan, K., Griffith, D., and Stevens, L.: Trace gas emissions from combustion of peat, crop residue, domestic biofuels, grasses, and other fuels: configuration and Fourier transform infrared (FTIR) component of the fourth Fire Lab at Missoula Experiment (FLAME-4), Atmospheric Chemistry and Physics, 9727, 2014.
Tuch, T. M., Haudek, A., Müller, T., Nowak, A., Wex, H., and Wiedensohler, A.: Design and performance of an automatic regenerating adsorption aerosol dryer for continuous operation at monitoring sites, Atmos. Meas. Tech., 2, 417-422, 2009.
van der Werf, G. R., Randerson, J. T., Giglio, L., Collatz, G., Mu, M., Kasibhatla, P. S., Morton, D. C., DeFries, R., Jin, Y. v., and van Leeuwen, T. T.: Global fire emissions and the contribution of deforestation, savanna, forest, agricultural, and peat fires (1997–2009), Atmospheric Chemistry and Physics, 10, 11707-11735, 2010.
Wang, X., Thai, P. K., Mallet, M., Desservettaz, M., Hawker, D. W., Keywood, M., Miljevic, B., Paton-Walsh, C., Gallen, M., and Mueller, J. F.: Emissions of selected semivolatile organic chemicals from forest and savannah fires, Environmental science & technology, 51, 1293-1302, 2017.
Whittlestone, S., and Zahorowski, W.: Baseline radon detectors for shipboard use: Development and deployment in the First Aerosol Characterization Experiment (ACE 1), Journal of Geophysical Research: Atmospheres, 103, 16743-16751, 1998.
Winton, V., Bowie, A., Edwards, R., Keywood, M., Townsend, A., van der Merwe, P., and Bollhöfer, A.: Fractional iron solubility of atmospheric iron inputs to the Southern Ocean, Marine Chemistry, 177, 20-32, 2015.
Winton, V., Edwards, R., Bowie, A., Keywood, M., Williams, A., Chambers, S., Selleck, P., Desservettaz, M., Mallet, M., and Paton-Walsh, C.: Dry season aerosol iron solubility in tropical northern Australia, Atmospheric Chemistry and Physics Discussions, doi:10.5194/acp-2016-419, 2016.
Wong, J., and Li, Z.: Retrieval of optical depth for heavy smoke aerosol plumes: uncertainties and sensitivities to the optical properties, Journal of the Atmospheric Sciences, 59, 250-261, 2002.
Yokelson, R. J., Crounse, J. D., DeCarlo, P. F., Karl, T., Urbanski, S., Atlas, E., Campos, T., Shinozuka, Y., Kapustin, V., Clarke, A. D., Weinheimer, A., Knapp, D. J., Montzka, D. D., Holloway, J., Weibring, P., Flocke, F., Zheng, W., Toohey, D., Wennberg, P. O., Wiedinmyer, C., Mauldin, L., Fried, A., Richter, D., Walega, J., Jimenez, J. L., Adachi, K., Buseck, P. R., Hall, S. R., and Shetter, R.: Emissions from biomass burning in the Yucatan, Atmospheric Chemistry and Physics, 9, 5785-5812, 2009.

990